J. Fluid Mech. (1986), *vol.* 164, *pp.* 155–183
Printed in Great Britain

Flow regimes in a circular Couette system with independently rotating cylinders

By C. DAVID ANDERECK†, S. S. LIU‡
AND HARRY L. SWINNEY
Department of Physics, The University of Texas, Austin, Texas 78712

(Received 20 December 1984 and in revised form 8 September 1985)

Our flow-visualization and spectral studies of flow between concentric independently rotating cylinders have revealed a surprisingly large variety of different flow states. (The system studied has radius ratio 0.883, aspect ratios ranging from 20 to 48, and the end boundaries were attached to the outer cylinder.) Different states were distinguished by their symmetry under rotation and reflection, by their azimuthal and axial wavenumbers, and by the rotation frequencies of the azimuthal travelling waves. Transitions between states were determined as functions of the inner- and outer-cylinder Reynolds numbers, R_i and R_o, respectively. The transitions were located by fixing R_o and slowly increasing R_i. Observed states include Taylor vortices, wavy vortices, modulated wavy vortices, vortices with wavy outflow boundaries, vortices with wavy inflow boundaries, vortices with flat boundaries and internal waves (twists), laminar spirals, interpenetrating spirals, waves on interpenetrating spirals, spiral turbulence, a flow with intermittent turbulent spots, turbulent Taylor vortices, a turbulent flow with no large-scale features, and various combinations of these flows. Some of these flow states have not been previously described, and even for those states that were previously described the present work provides the first coherent characterization of the states and the transitions between them. These flow states are all stable to small perturbations, and the transition boundaries between the states are reproducible. These observations can serve as a challenge and test for future analytic and numerical studies, and the map of the transitions provides several possible codimension-2 bifurcations that warrant further study.

1. Introduction

There has been a very large number of experimental and theoretical studies of flow between concentric rotating cylinders (circular Couette flow) in the century since the earliest studies were conducted by Mallock (1888, 1896) and Couette (1890). Most of the work has concerned the primary instability, but in recent years some studies have examined the instabilities that occur at higher cylinder-rotation rates. The present study was designed to explore systematically the flow states that occur over a large range of rotation rates of the inner and outer cylinders in a circular Couette system, and to examine the transitions between the different states.

The Navier–Stokes equations for flows far from equilibrium of course have in general multiple stable solutions. A graphic demonstration of this non-uniqueness was provided by Coles' (1965) discovery that, depending on the path followed in

† Present address: Department of Physics, The Ohio State University, Columbus, Ohio 43210.
‡ Present address: Research and Teaching Section of Physics, Department of Basic Sciences, Tianjin University, People's Republic of China.

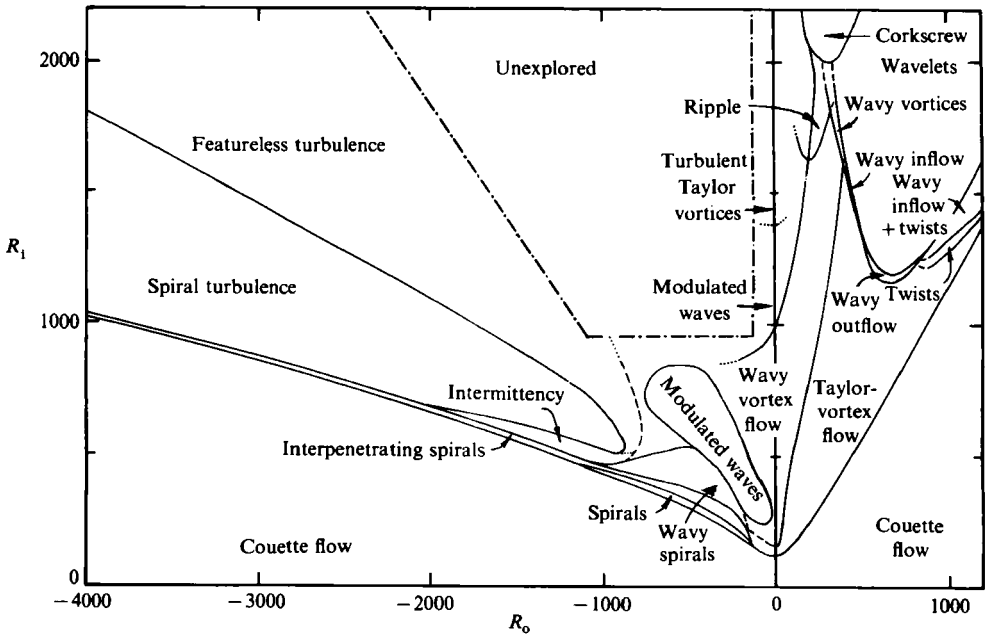

FIGURE 1. Regimes observed in flow between independently rotating concentric cylinders. Dashed lines indicate the transition boundaries that are difficult to establish from visual observation alone since there is no abrupt change in the appearance. Dotted lines indicate the expected, but not yet observed, continuation of several boundaries. More detail is shown in figures 2 and 18 for counter-rotating and co-rotating cylinders, respectively.

parameter space, up to 26 distinct stable flow states could be obtained at the same Reynolds number in his circular Couette system. Therefore, in a study such as the present one a well-prescribed path in parameter space must be followed if the experiments are to serve as a useful guide to future theoretical and experimental studies. The procedure we have followed is a natural one for numerical, analytical, and experimental studies. First the outer cylinder is slowly accelerated from rest to its final rotation rate with the inner cylinder at rest; this yields the laminar azimuthal flow (Couette flow). Then the inner cylinder is slowly (quasi-statically) accelerated from rest to its final rotation rate. This well-defined straightforward protocol follows what is sometimes called in bifurcation theory a 'thermodynamic path' away from thermodynamic equilibrium ($R_i = R_o = 0$). The same protocol was followed in the experiments of Coles (1965), Snyder (1968*a*, *b*, 1970), and Andereck, Dickman & Swinney (1983). In some cases we deviated from this protocol when it was found that a particular state could be produced more rapidly by an alternative method (see §3).

The principal result of this study is the surprisingly complex transition diagram shown in figure 1; the different flows, some of which have not been previously described, are listed in table 1. The different flows have been distinguished in the experiments by their axial and azimuthal wavenumbers, symmetry under reflection (about a plane normal to the cylinder axis), and the rotation frequencies of the different modes. The transitions at low Reynolds numbers in figure 1 are accessible in numerical simulations with currently available computers, so it should be possible in future combined experimental–numerical studies to gain insight into the physical mechanisms responsible for the transitions identified in figure 1. In addition, the

AZI = azimuthal laminar flow with weak Ekman vortices
CKS = corkscrew
INT = intermittent turbulent spots
IPS = interpenetrating spirals
MWV = modulated wavy vortices
RIP = ripple
SPI = spiral vortices
SPT = spiral turbulence
TRA = transition region
TTV = turbulent Taylor vortices
TUR = turbulent flow (featureless)
TVF = Taylor vortex flow
TWI = twisted vortices
WIB = wavy inflow boundary
WIS = wavy interpenetrating spirals
WOB = wavy outflow boundary
WVF = wavy vortex flow
WVL = wavelets

TABLE 1. The principal regimes observed in flow between independently rotating cylinders

junctions of the transition curves can be studied by bifurcation theory (normal forms in codimension-2 theory). The transitions at larger Reynolds numbers should serve as a guide for later theoretical and numerical work.

The remainder of this section defines the parameters of a circular Couette system. Section 2 reviews previous work, and §3 describes the procedure used to obtain the flow states we have studied. Sections 4 and 5 present, respectively, our results obtained for counter-rotating and co-rotating cylinders. Section 6 contains concluding remarks.

A circular Couette system with both cylinders rotating is characterized by the following control parameters: the radius ratio $\eta = a/b$, where a and b are the inner- and outer-cylinder radii; the aspect ratio $\Gamma = L/(b-a)$, where L is the length of the fluid column; the inner- and outer-cylinder Reynolds numbers $R_i = a(b-a)\,\Omega_i/\nu$ and $R_o = b(b-a)\,\Omega_o/\nu$, where Ω_i (Ω_o) is the angular velocity of the inner (outer) cylinder and ν is the kinematic viscosity; and the end conditions. Our system, discussed in Andereck *et al.* (1983), has $a = 5.250$ cm and $b = 5.946$ cm, giving $\eta = 0.883$. Our flow-regime diagrams were obtained primarily for $\Gamma = 30$; Teflon rings attached to the outer cylinder defined the upper and lower boundaries. The parameter values chosen are typical of those used in several previous experiments.

Some measurements were also made with Γ ranging from 20 to 48 (with both free and fixed upper surfaces); in the range $-1500 < R_o < 0$ no aspect ratio dependence of the transition boundaries was discerned, so data for different aspect ratios were combined. Furthermore, in *no* case was the existence of a particular type of flow found to depend on the aspect ratio. However, the fluid behaviour can be quantitatively different for other values of Γ (King & Swinney 1983; King *et al.* 1984).

Since the state of the system is generally not uniquely determined by the values of η, Γ, R_i and R_o (except near thermodynamic equilibrium), the complete specification of a flow state must include properties such as the number of Taylor vortices N and the wavenumbers m_i of azimuthal modes as well as the external control parameters.

2. Previous work

Several experimental investigations have been reported on the flows between independently rotating cylinders; however, until very recently there has been relatively little theoretical work on the problem. Taylor (1923) investigated theoretically and experimentally the stability of azimuthal Couette flow with both cylinders rotating. He studied in detail only the onset of axisymmetric Taylor vortices. Coles (1965) found that the azimuthal flow between counter-rotating cylinders was (for sufficiently large $|\Omega_0/\Omega_1|$) unstable to non-axisymmetric spiral vortices. In his monumental study of flows between both counter- and co-rotating cylinders Coles discovered several very distinctive flows, including intermittent turbulent bursts and spiral turbulence. Van Atta (1966) reported extensive hot-wire anemometer measurements of spiral turbulence. Snyder (1968*a*, *b*) made detailed comparisons of his observations of the most unstable wavenumber of spiral vortices between counter-rotating cylinders with the predictions of Krueger, Gross & DiPrima (1966). Snyder (1970) found, for $\eta = 0.2$, 0.5, 0.8 and 0.959, a variety of waveforms occurring for small R_0 in both counter- and co-rotating cylinders. Snyder (1969) also found that the finite length of the cylinders and the specific boundary conditions at the ends of the fluid column are important in determining how near a given system is to the ideal infinite-cylinder case. In particular, he showed that the penetration of the Ekman-pumped cells into the bulk of the fluid can affect the flow, a point we will discuss in §§4.1 and 5.1. Jones (1982) studied numerically the flow between counter-rotating cylinders for small R_0; we will discuss his results in §4.3. Finally, Andereck *et al.* (1983) have reported the observation of five new flows occurring between co-rotating cylinders. The present study surveys the flows occurring between counter-rotating cylinders and extends our earlier work on co-rotating cylinders.

3. Experimental procedures

Visualization of the flow states was accomplished using a mixture of 2% by volume Kalliroscope AQ1000 in water (Matisse & Gorman 1984). The presence of Kalliroscope, an aqueous suspension of $25 \times 6 \times 0.07$ μm polymeric flakes, increases the effective fluid viscosity by about 2%. Interpretation of photographs of flow visualized with polymeric flakes is based on the following: a dark area indicates flow along the observer's line of sight, while a light area indicates flow perpendicular to the line of sight. For a detailed discussion, see Savaş (1985).

We have made some of our measurements with the system immersed in a water bath with temperature control of ± 0.01 °C, but most measurements were made without temperature control; however, the temperature in our laboratory varied by only about 0.1 °C over the course of a given transition-sequence run, and the same results were obtained with and without precision temperature control.

Time dependences of the flows have been studied by measuring the intensity of laser light scattered by the flakes, as described in Andereck *et al.* (1983). Power spectra obtained from time-series records of intensity were used to determine angular velocities of the various flow features and to distinguish periodic or multiply-periodic flows from non-periodic flows.†

The first step in locating the flow transition boundaries by the protocol described in §1 was the determination of what constituted an 'adiabatic' acceleration of the

† All frequencies in the power spectra are scaled as ω/Ω_1.

inner cylinder. Measurements were initially made for a wide range of acceleration rates, and it was found that within the experimental uncertainty (about 2 %) no shifts in the transition boundaries were discernible for average angular accelerations less than 0.15 rad/min^2; hence the transition boundaries were traversed with acceleration rates less than or equal to this value. Future studies designed to examine with the highest precision possible any of the particular transition boundaries that we have discovered will of course have to be conducted with even smaller acceleration rates [cf. Park, Crawford & Donnelly (1981); Ahlers, Cannell & Dominguez-Lerma (1983) for detailed studies of the Taylor instability and wavy vortex flow, respectively]. However, it is unlikely that the properties of the different flow states (symmetries, wavenumbers, frequencies) will be altered by smaller acceleration rates from rest. For example, Andereck *et al.* (1983) found that transitions from Taylor-vortex flow, studied by adiabatic acceleration of the inner cylinder, were independent of the way in which the flow was produced.

4. Flow between counter-rotating cylinders

The transitions observed in flow between counter-rotating cylinders are summarized in figure 1 and are shown in greater detail for small Reynolds numbers in figure 2.

4.1. *Basic flow and Ekman cells*

The basic flow (Couette flow) between infinitely long cylinders is azimuthal with magnitude given by $Ar+B/r$, where

$$A = -\Omega_1(\eta^2-\mu)/(1-\eta^2), \quad B = \Omega_1 a^2(1-\mu)/(1-\eta^2),$$

and $\mu = \Omega_0/\Omega_1$. The fluid velocity vanishes on a cylinder of radius

$$r = a[(1-\mu)/(\eta^2-\mu)]^{\frac{1}{2}}.$$

In a finite system the pumping of fluid into the Ekman layers adjacent to the top and bottom boundaries introduces a non-azimuthal circulation that may be significant under some conditions. This circulation, studied by Coles & Van Atta (1966) and Snyder (1969), takes the form of large, relatively weak, horizontal vortices that may extend from each end to the mid-plane of the system, depending on R_0 and R_1. This is the flow designated AZI in figure 2. For the counter-rotating case in a system with $\Gamma = 29$, $\eta = 0.5$, and rigid upper and lower boundaries attached to the outer cylinder, Snyder found that for $R_0 = -120$, $R_1 = 100$ there were 4 large vortices present, 2 near the outer cylinder and 2 near the inner cylinder. The azimuthal velocity measurements of Coles & Van Atta (for $R_1 = 0$ and $R_0 = 3000$, 6000 and 9000) show a distortion of the $Ar+B/r$ velocity profile near the mid-plane for $\Gamma \simeq 27$ and $\eta = 0.889$. They conclude, however, that the radial and axial components are very small. Nevertheless, the Ekman cells can be detected in our system when the outer cylinder is spun at high speed after the system has been at rest for a few hours to allow the Kalliroscope flakes to sediment, as figure 3 (*a*) illustrates. The flakes then mix with the fluid below the mid-plane but do not penetrate above it.

There is some indication that the Ekman cells persist in the presence of strong secondary flows; for example, a thin dark line is sometimes seen marking the location of the mid-plane, and evidently the Ekman cell boundaries, in the laminar spiral vortex flow. The strength of the interaction between the Ekman cells and other modes is not known but is probably weak for large Γ.

Finite-length effects, such as the vortex-size quantization condition found by Park

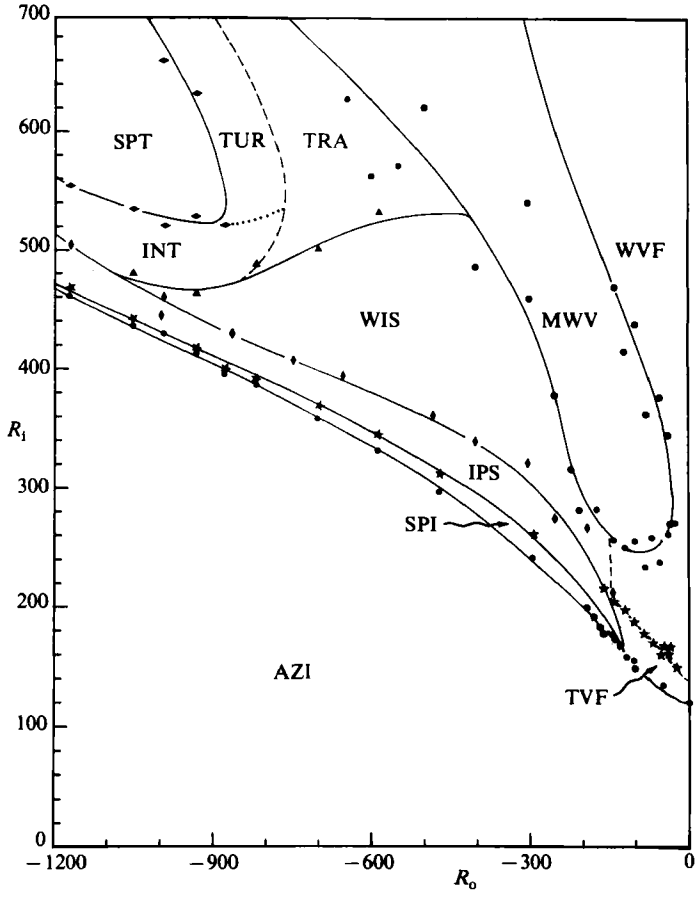

FIGURE 2. The flow-regime diagram for counter-rotating cylinders. The abbreviations for the different flows are defined in table 1. The different symbols distinguish data for different transitions.

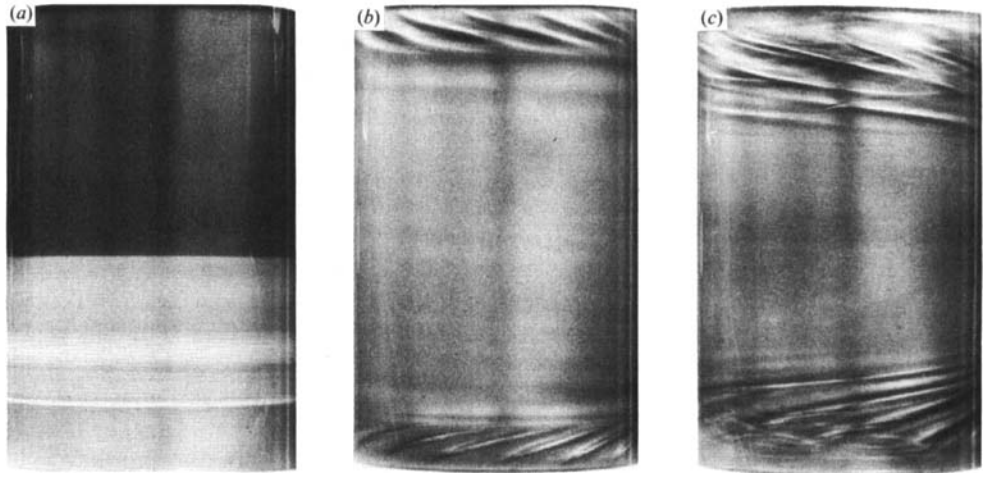

FIGURE 3. End effects. Inner cylinder at rest: (*a*) $R_o = 1000$, $R_i = 0$; Kalliroscope flakes fill only the lower half of the cylinder as it is spun up from rest. Co-rotating cylinders: (*b*) $R_o = 1000$, $R_i = 1124$; (*c*) $R_o = 4005$, $R_i = 4520$.

& Donnelly (1981), may affect slightly the location of some of the transition boundaries that we observe, although the basic behaviour found here should not be significantly affected.

4.2. *Primary instabilities*

When $R_o > -155 \pm 10$ the basic flow is unstable to time-independent axisymmetric Taylor-vortex flow; see the region labelled TVF in figure 2. If $R_o < -155$ (region SPI of figure 2), the basic flow is centrifugally unstable to non-axisymmetric spiral vortices near the inner cylinder (Coles 1965; Krueger, Gross & DiPrima 1966; Snyder 1968*a*, *b*). We have examined the radial cross-section of the flow using the slit-illumination technique of Snyder (1968*a*) and have found that the spirals are approximately confined to this unstable region. The primary pattern that forms is shown in figure 4(*a*), where two spirals exist separated by an interface located near the mid-plane. The interface location is not always constant with time, nor is it necessarily as well defined as in the photograph; sometimes the interface region is 2 to 3 times the size of the vortices and consists of the overlap of both of the originally separate spirals. For the particular case shown in the figure the lower spiral eventually left the flow completely, leaving the upper spiral over the entire annulus, as shown in figure 4(*b*).

Near $R_o = -155$, Taylor or spiral vortices are weakly stable; they can in fact exist simultaneously in different regions of the cylinder system. Increasing R_i leads to a complicated series of transitions from Taylor-vortex flow to spirals and mixtures of the two flows. The order of these transitions is not well established and may depend sensitively on initial conditions, boundary conditions, and the external noise level.

The time dependence of spiral-vortex flow can be complex; figure 4(*c*) shows a time series for light scattered from near the mid-plane for a state at Reynolds numbers slightly higher than those for the photographs. The changes in the character of the interface with time lead to a power spectrum with broad components (figure 4*d*), indicating that there is an unpredictable element in the flow. This is in marked contrast with the first time-dependent flow for $R_o = 0$, wavy-vortex flow, which is periodic over a large range of R_i and vortex sizes. It is not clear why there should be a difference in the dynamics; infinite-cylinder theories may not show such behaviour since the non-periodicity could be related to the presence of the top and bottom boundaries. If the end boundaries were not perfectly aligned perpendicular to the rotation axis, one might expect a periodic forcing of the flow, not the non-periodic behaviour observed. On the other hand, if the location of the interface is determined by a delicate balance between Ekman pumping occurring at either end, it may simply be very sensitive to any mechanical perturbations of the system, resulting in a wandering or diffuse interface. In addition, small temperature gradients in the flow might induce the observed non-periodicity.

For $R_o < -1500$, separate spirals exist in our system only as short-lived transients. Within a few seconds after their formation the interface between the spirals breaks down, if it has ever developed, allowing the two spirals to interpenetrate and thereafter co-exist over most of the cylinder length (see §4.5).

4.3. *Wavy-vortex flow*

The wavy-vortex flows found in the region labelled WVF in figure 2 are similar in many respects to wavy-vortex flows with $R_o = 0$ except that the number of azimuthal waves is typically larger (8 or 9) with counter-rotating cylinders than with the outer

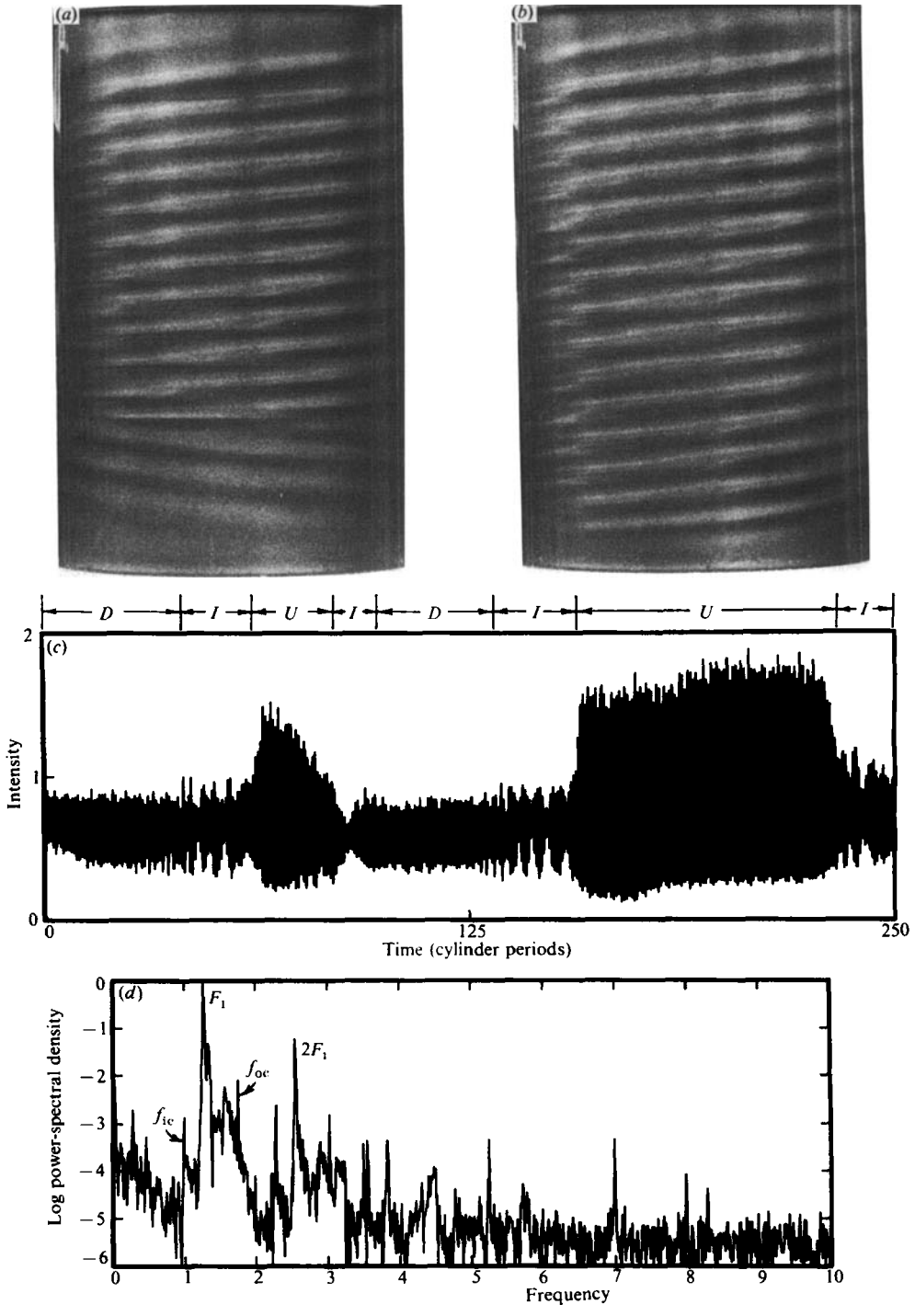

FIGURE 4. Laminar spiral flow (SPI): (*a*) Separate laminar spirals, $R_o = -300$, $R_i = 240$. (*b*) Single laminar spiral, $R_o = -300$, $R_i = 240$. (*c*) The time dependence of scattered light intensity for $R_o = -690$, $R_i = 350$, where U, D, and I indicate respectively an upward-moving spiral, downward-moving spiral, and interpenetrating spirals. (*d*) The power spectrum for $R_o = -690$, $R_i = 350$. (f_{oc} and f_{ic}, the frequencies of the inner and outer cylinders respectively, are presumably artifacts arising from light reflected by the inner and outer cylinder walls.)

Γ	R_o	R_i	μ	Ta	α	m	ω_e (experiment)	ω_c (Jones 1982)
30	−96	167	−0.51	5733	3.56	2	0.280	0.242
30	−119	170	−0.62	6459	3.56	2	0.280	0.204
30	−125	187	−0.59	7642	3.77	2	0.245	0.135
30	−158	230	−0.60	11707	3.77	6	0.143	0.058
30	−152	223	−0.60	10928	3.56	7	0.136	0.050
20	−153	223	−0.60	10987	3.77	7	0.141	0.050

TABLE 2. A comparison of the measured angular velocities of the waves with the predictions of Jones (1982) for wavy-vortex flow between counter-rotating cylinders. Ta is the Taylor number, α is the dimensionless axial wavenumber [$\alpha \equiv 2\pi(b-a)/\lambda$, where λ is the vortex axial wavelength], m is the azimuthal wavenumber, and the angular velocities ω_e and ω_c are expressed relative to the inner-cylinder frequency.

cylinder at rest (usually 7 or fewer waves). As shown in table 2, we have measured the angular velocities for a few cases, and have compared them with the predictions of Jones (1982). The agreement between experiment and theory is good at small Taylor numbers ($Ta \equiv 2\Omega_i^2 d^4(\eta^2-\mu)/(1-\eta^2)\nu^2$), but the difference between theory and experiment becomes large at larger Taylor numbers. However, the calculations are not expected to apply if the waves redistribute angular momentum significantly, and that appears to be the case at larger Taylor numbers (C. A. Jones, private communication).

4.4. *Low-R_i modulated wavy-vortex flow*

The closed region labelled MWV in figure 2 consists of modulated waves on Taylor vortices, similar in nature to the flows with two travelling waves on Taylor vortices studied with $R_o = 0$ (Gorman & Swinney 1982; Shaw *et al.* 1982). However, the region of occurrence is in a much lower range of R_i than the MWV regime for $R_o = 0$.

One of the important features of these flows is the lack of phase-locking between waves on different Taylor vortices, illustrated in figure 5. Waves on different Taylor vortices oscillate azimuthally with respect to one another, as viewed in a reference frame moving at the mean angular velocity of the waves. The amplitude of these oscillations is about one-half of an azimuthal wavelength, and the axial wavelength is comparable with the length of the cylinders. This oscillation produces a third component in the spectra, as seen in figure 6, with frequency considerably lower than the two primary components that correspond to the wave-rotation frequency and its modulation frequency. This oscillation may arise from a non-propagating mode, although this is difficult to determine without the benefit of further measurements in a rotating reference frame. Zhang & Swinney (1984) have found non-propagating modes when $R_o = 0$.

Finally, the amplitude of the modulation is large; at maximum modulation the wave in question virtually disappears. In contrast, for $R_o = 0$ the waves flatten without losing their basic form.

4.5. *Interpenetrating laminar spirals*

The interface between the spirals in the upper and lower portions of the annulus (discussed in §4.2) disappears as R_i is increased, allowing both spirals to exist simultaneously over most of the cylinder length. These interpenetrating spirals are

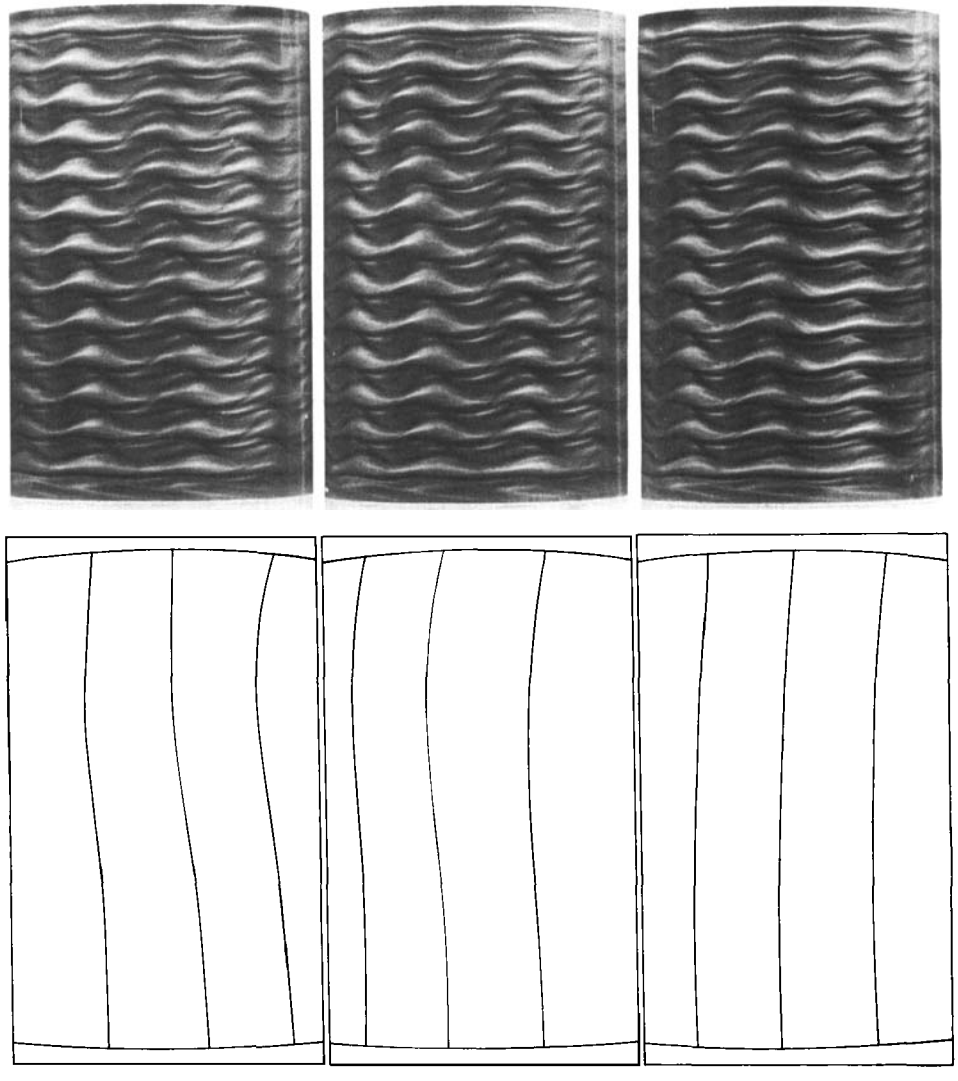

FIGURE 5. Modulated wavy vortex flow (MWV) at $R_o = -100$, $R_i = 350$. The time interval between photographs is 10.0 s; the period of the inner cylinder is 7.22 s, the outer cylinder, 28.7 s. The line drawings indicate the location of wave crests.

found in the region marked IPS in figure 2. Near each end of the cylinder system only one of the spirals exists, the one that existed in that end of the system in the separate spiral state. Such a flow is shown in figure 7, where a comparison is made between the appearance at low and high outer-cylinder speeds. The spiral vortices are distinctly smaller for $R_o = -3000$; the size difference correlates with the thickness of the centrifugally unstable layer next to the inner cylinder, which is proportional to Ω_i/Ω_o for $\Omega_o \gg \Omega_i$. When viewed in a cross-section the two spirals are not found to be separated radially, with one near the inner cylinder and the other near the outer cylinder, but instead both are approximately confined to the unstable layer near the inner cylinder.

Figure 7 also shows power spectra corresponding to the photographed states. At

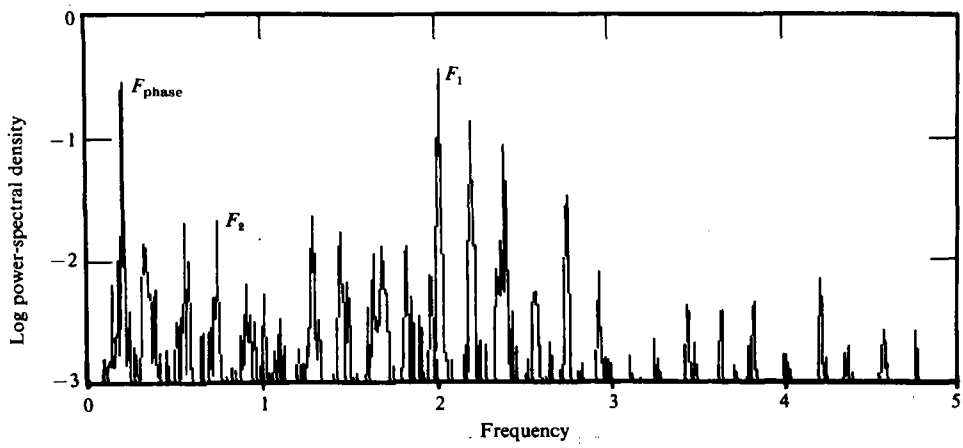

FIGURE 6. Power spectrum of low-R_i modulated wavy-vortex flow (MWV); $R_o = -110$, $R_i = 350$, F_1 is the rotation frequency of the wavy pattern, F_2 is the modulation frequency, and F_{phase} is the frequency of axial phase oscillation.

low R_o there is one reasonably well defined frequency associated with the flow, along with harmonics, although much of the spectral power is concentrated in the broad peaks. At high R_o there are no traces of sharp components left; the only peaks aside from instrumental artifacts are very broad. Thus, although the interpenetrating spirals appear visually to have a nearly ordered spatial structure, the spectra indicate that the pattern is continuously evolving in a non-periodic way.

4.6. *Wavy interpenetrating spirals*

In the region labelled WIS in figure 2, the interpenetrating laminar spirals are unstable to the formation of waves. Typically these states, as shown in figure 8, are not as well defined visually as wavy-vortex flow. The visual appearance is time-dependent; for constant R_o and R_i the wavy structure may be quite evident for a while, then a short time later the appearance is similar to the interpenetrating laminar spirals. The spectra of these flows are lacking in features, with only a noisy background present that increases in power at low frequencies.

4.7. *Intermittency*

Turbulent spots form in interpenetrating laminar spiral flow in the region marked INT in figure 2. Figure 9 is a sequence of photographs of such a flow. The time evolution is apparently non-periodic, with spots forming and decaying at random locations in the flow with a timescale of the order of a few outer-cylinder periods. The spots vary in size from 2 to 20 times the width of the gap between the cylinders. With R_i near the lower boundary of the region of occurrence the spots form as the laminar spirals decrease in intensity, and then disappear as the spirals build to their former strength. Near the upper boundary of the region the laminar spirals are much weaker, and the spots are more persistent.

A typical time-series record of the reflected-light intensity for this flow is shown in figure 10 (*a*). The corresponding power spectrum, shown in figure 10 (*b*), has no sharp features. Figure 10 (*b*) shows that over much of the frequency range the spectral power apparently drops off exponentially fast, consistent with deterministic non-periodic behaviour (Frisch & Morf 1981; Greenside *et al.* 1982), while figure 10 (*c*) indicates a possible power-law decrease, consistent with stochastic models of noise (Greenside

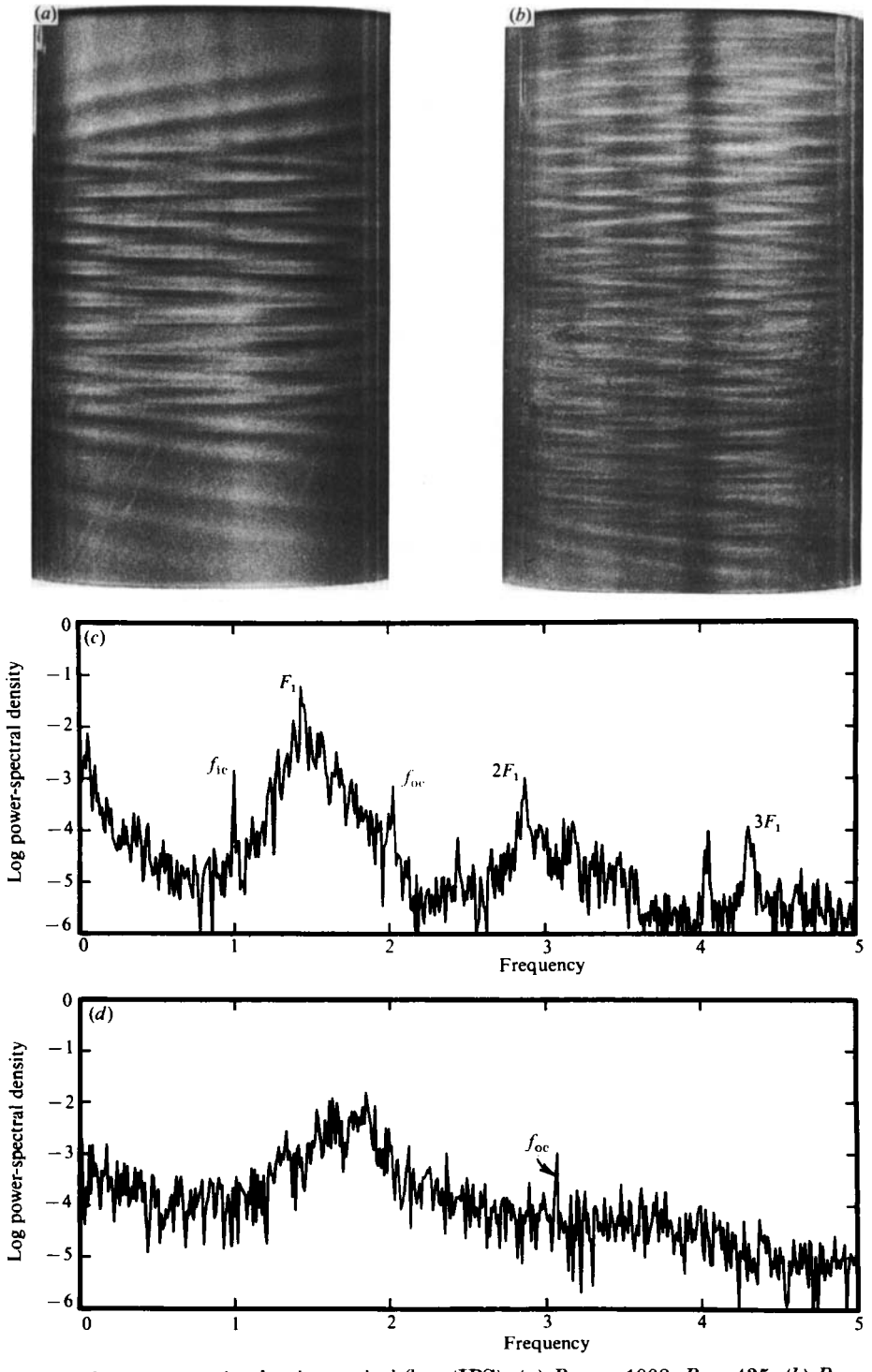

FIGURE 7. Interpenetrating laminar spiral flow (IPS): (*a*) $R_o = -1000$, $R_i = 435$; (*b*) $R_o = -3000$, $R_i = 860$; (*c*) power spectrum of (*a*); (*d*) power spectrum of (*b*).

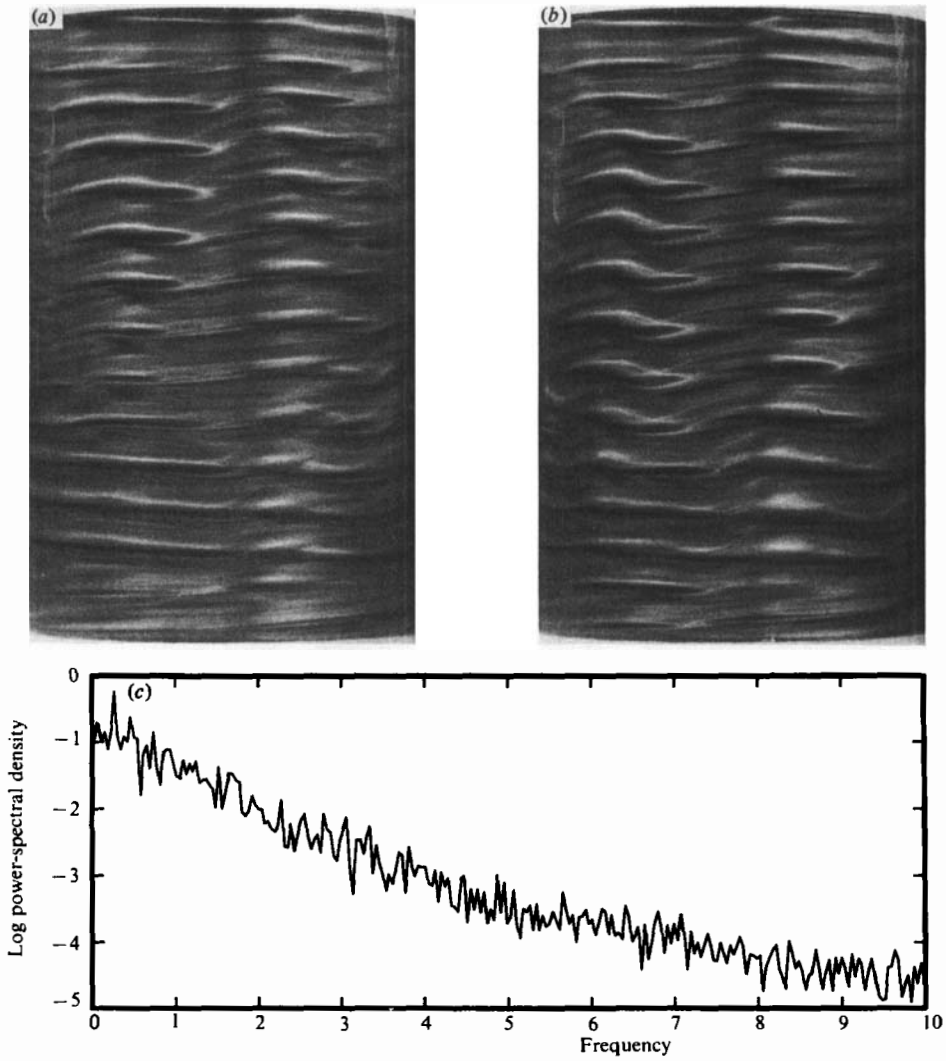

FIGURE 8. Wavy interpenetrating spiral flow (WIS): (*a*) and (*b*) show two successive views of the same flow at $R_o = -300$, $R_i = 350$. (*c*) Power spectrum of this flow.

et al. 1982). Owing to this ambiguity we can draw no conclusion as to the nature of the noise in this flow.

4.8. *Transition region*

The region labelled TRA in figure 2 consists of an ill-defined flow regime in which transition occurs between intermittent turbulent-spot formation, turbulent flow, wavy interpenetrating spirals, and modulated wavy Taylor vortices. The detailed behaviour in this region has not been studied, but should be very interesting since a large variety of flows are competing for stability.

4.9. *Spiral turbulence*

Spiral turbulence, which consists of a periodic alternation of spiral turbulent and laminar bands, exists in the region labelled SPT in figure 2. A photographic sequence

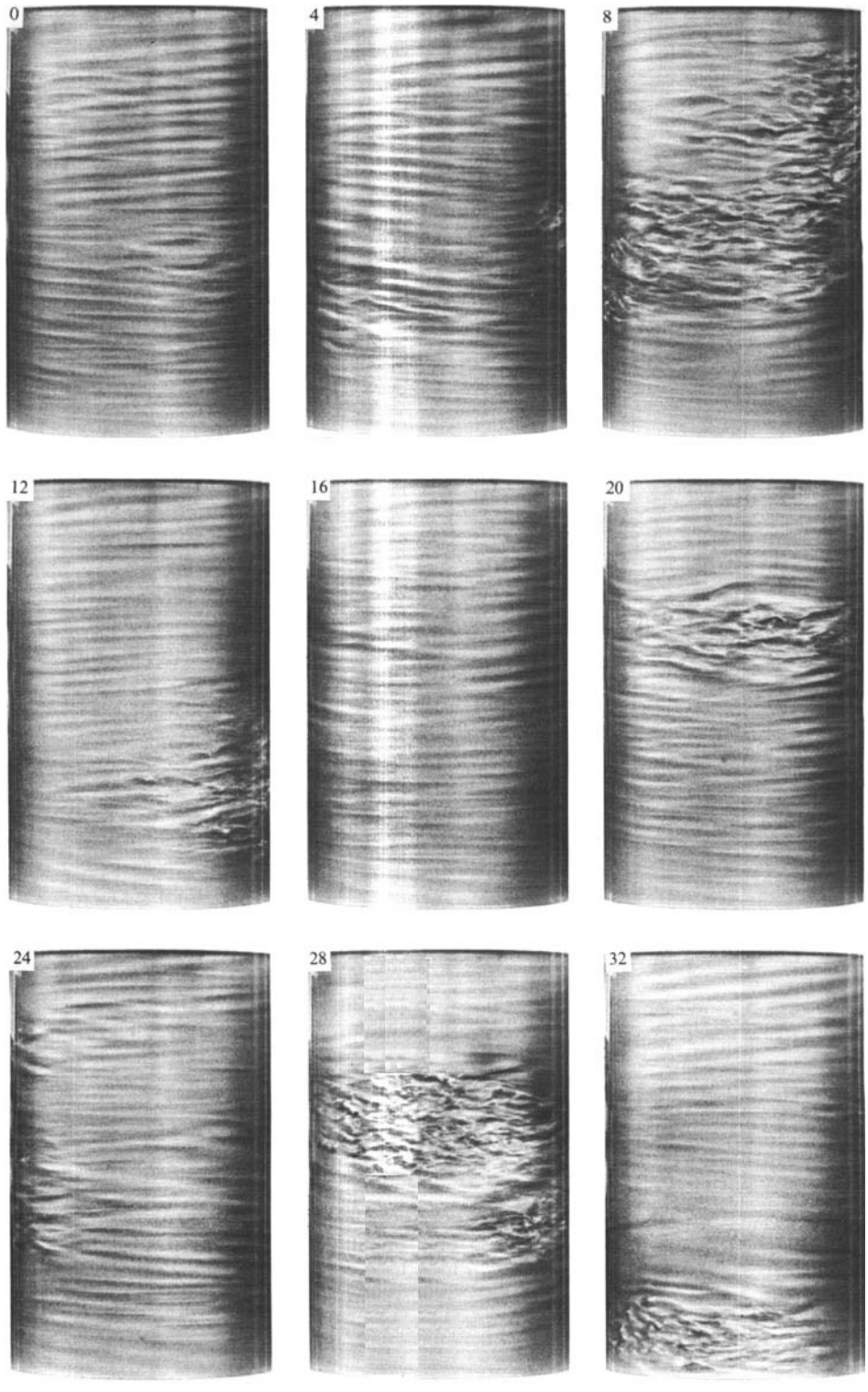

FIGURE 9. Intermittent turbulent spots (INT) in a flow with interpenetrating laminar spirals. The numbers labelling the photographs give the time in seconds; the period of the inner cylinder was 4.25 s, the outer cylinder, 1.87 s ($R_o = -1500$, $R_i = 590$).

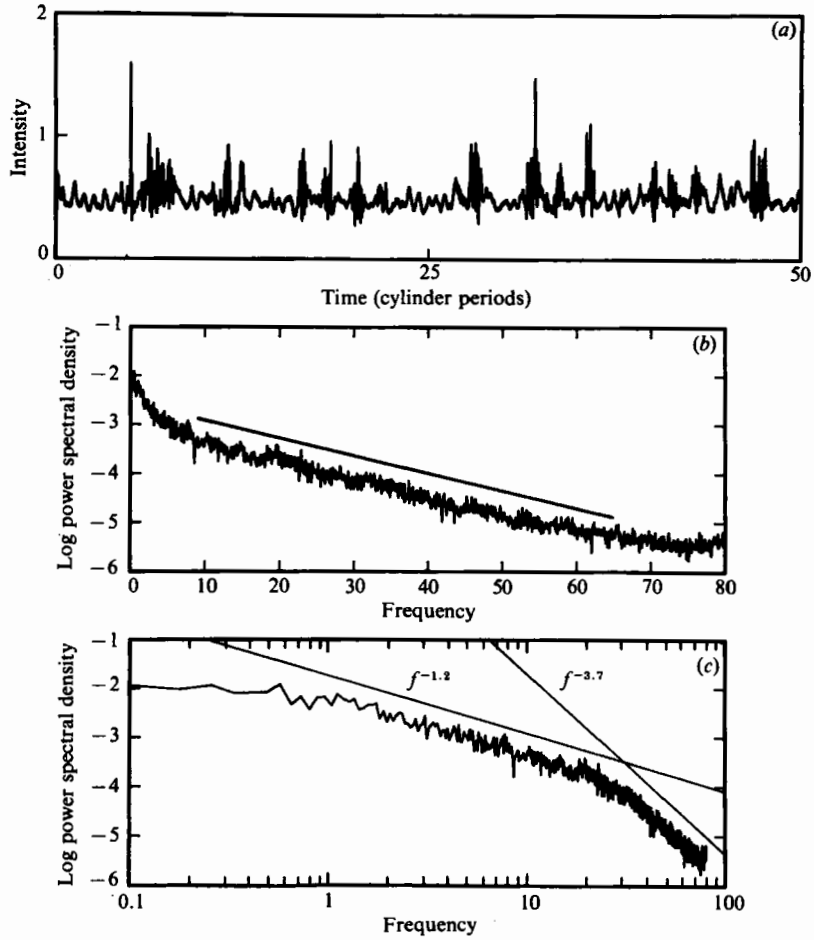

FIGURE 10. (*a*) Reflected-intensity time series for a flow with intermittent turbulent spots for $R_o = -1500$, $R_i = 590$. (*b*) A semi-log power spectrum of the state in (*a*); for comparison the solid straight line shows a pure exponential decay. (*c*) A log–log-scale power spectrum of the state in (*b*). The slight rise in the spectral power at the highest frequencies is due to aliasing (Otnes & Enochson 1978). See text for a discussion of the spectra.

of a typical state of spiral turbulence is shown in figure 11. Both right- and left-handed spirals were observed, although the relative probability of their occurrence was not determined. The power spectrum consists of a sharp frequency component, corresponding to the periodic passage of the turbulent band, and a broad noise background, as shown in figure 11 (*c*).

The rotation frequency ω_s of the spiral pattern has been studied by Coles (1965) and Van Atta (1966) over a wide range of cylinder speeds for large outer-cylinder rotation rates. They found the pattern moved with approximately the mean angular velocity of the two cylinders, although for $R_o \geqslant -10000$ the velocity differed significantly from the mean cylinder speed. We have measured ω_s (with $|R_o|$ much smaller than in the studies of Coles and Van Atta) and have found that ω_s/Ω_o is essentially constant over a large range of Ω_i (see figure 12).

When the system is in a laminar azimuthal flow state at sufficiently large $|R_o|$, a rapid increase in R_i to just above the lower boundary for spiral turbulence often

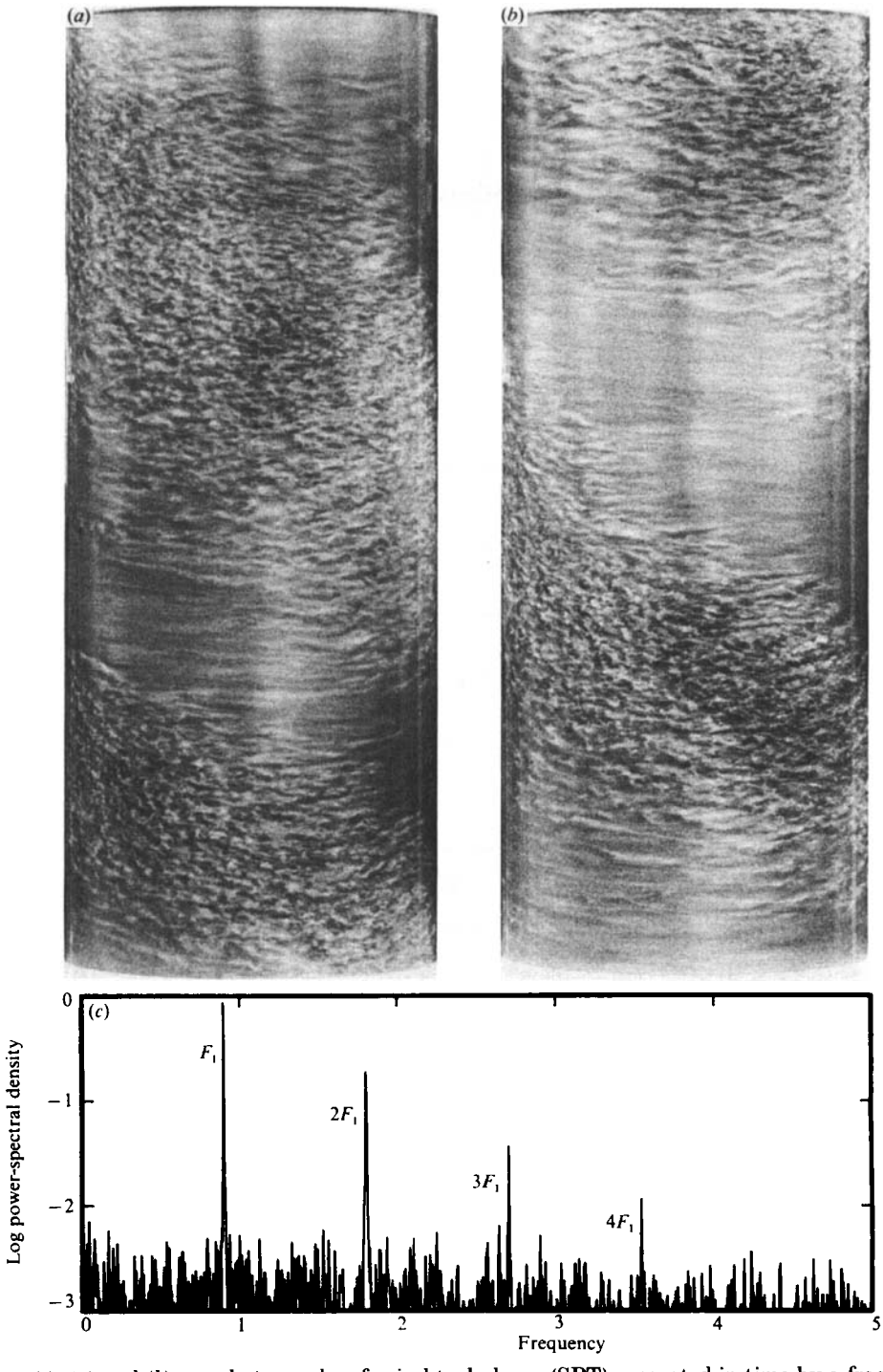

FIGURE 11. (*a*) and (*b*) are photographs of spiral turbulence (SPT) separated in time by a fraction of an inner-cylinder period; the period of the inner cylinder was 2.49 s, the outer cylinder, 0.81 s ($R_o = -3500$, $R_i = 1000$, $\Gamma = 48$). (*c*) Power spectrum of a nearby state ($R_o = -3000$, $R_i = 1000$, $\Gamma = 48$).

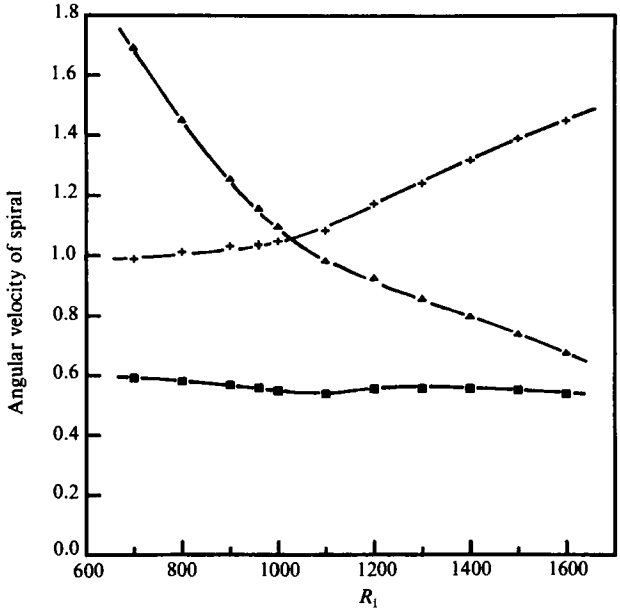

FIGURE 12. Spiral turbulence (SPT) pattern angular velocity as a function of R_i with fixed $R_o = -3500$. Some values were obtained in the hysteresis region below $R_i = 960$. ▲ indicates ω_s/Ω_i, + indicates $\omega_s/\bar{\Omega}$, where $\bar{\Omega} = \frac{1}{2}(\Omega_i + \Omega_o)$, and ■ indicates ω_s/Ω_o.

produces a state consisting of both-handed turbulent spirals, one in the upper half of the cylinder, the other in the lower half. The spirals join near the mid-plane to form a V-shaped pattern, as shown in the time-lapsed photographic sequence in figure 13. The location of the interface between the spirals may be related to the presence of Ekman cells. At large R_o this state can exist for many hours, perhaps indefinitely, but usually at low R_o it will decay after a few minutes to one or the other of the basic spirals.

As R_i increases, the width of the turbulent spiral band increases until finally there is no trace of a large-scale structure remaining, as the sequence of photographs in figure 14 illustrates. The corresponding spectra contain sharp components over a very large range in R_i, even persisting when the turbulent fraction approaches 1.

4.10. *Turbulent flow*

In spiral turbulence the fraction of turbulent fluid reaches 1 as R_i is increased. We call the resultant featureless flow turbulent. This flow, labelled TUR in figure 2, lacks any apparent large-scale structure, the dominant visible lengthscale being smaller than the gap between the cylinders for large cylinder speeds (see figure 15). However, at much larger R_i than the range shown in figures 1 and 2, a Taylor-cell-like structure re-emerges. (A region with weakly turbulent Taylor vortices (TTV) is shown in figures 1 and 18 for $R_o = 0$. This flow is discussed in Fenstermacher, Swinney & Gollub (1979) and Brandstater *et al.* (1983).) The power spectra for turbulent flow are featureless with a high frequency drop-off that is not inconsistent with a power law, although as in the case of intermittency we can draw no firm conclusion about the spectral behaviour at high frequencies.

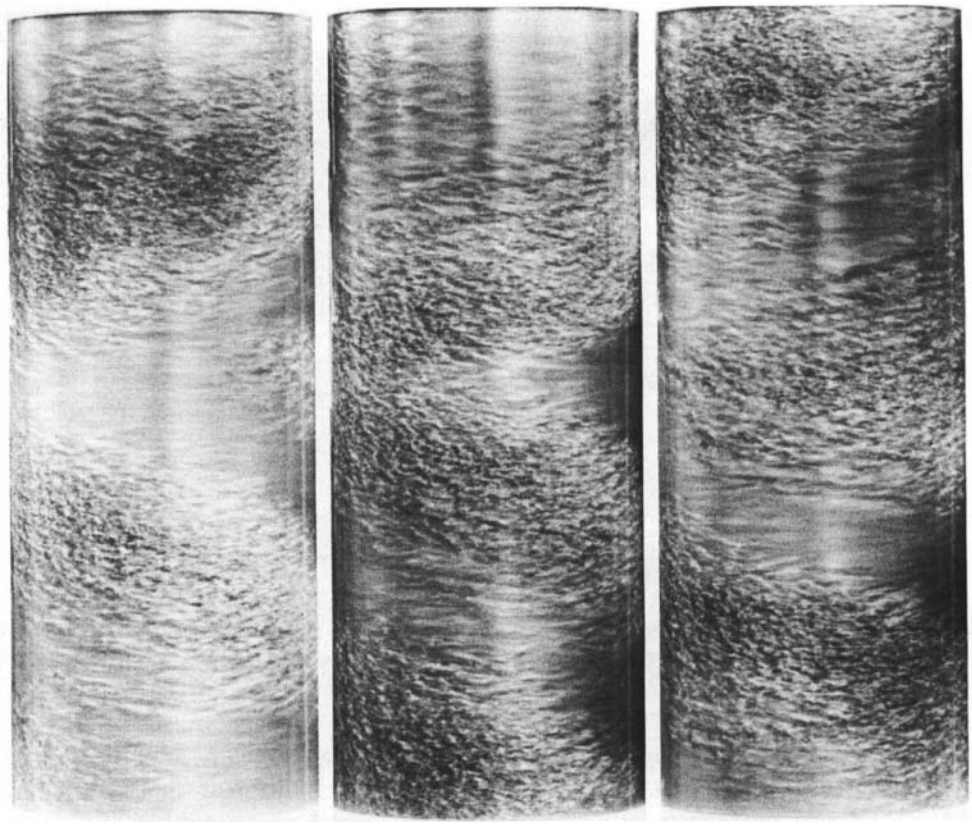

FIGURE 13. V-shaped turbulence for $R_o = -4670$, $R_i = 1070$, and $\Gamma = 48$. The time interval between photographs was a fraction of an inner-cylinder period; the period of the inner cylinder was 2.30 s, the outer cylinder, 0.60 s.

4.11. *Hysteresis*

Several of the flows between counter-rotating cylinders exhibit hysteresis in the locations of their stability boundaries in Reynolds-number space. We have limited our study of hysteresis to three flows: spiral turbulence (shown by Coles (1965) to be highly hysteretic), interpenetrating laminar spirals, and modulated wavy vortices. The results are summarized in figure 16. For each measurement R_o was fixed, R_i was increased to just beyond the stability boundary of interest, and then R_i was slowly decreased until the original flow was regained.

The magnitude of the hysteresis of spiral turbulence can be quite large, while for interpenetrating laminar spirals and modulated wavy vortices it is typically less than 10%. The hysteresis is large enough (for $R_o < -2000$) that at least three distinct flows are possible for given R_o and R_i, the flow actually realized depending on the system history.

Figure 17 illustrates the gradual change in a spiral turbulence pattern as R_i was decreased through the hysteresis regime. At $R_i \sim 690$, just below the last flow shown, the system returned abruptly to laminar azimuthal flow.

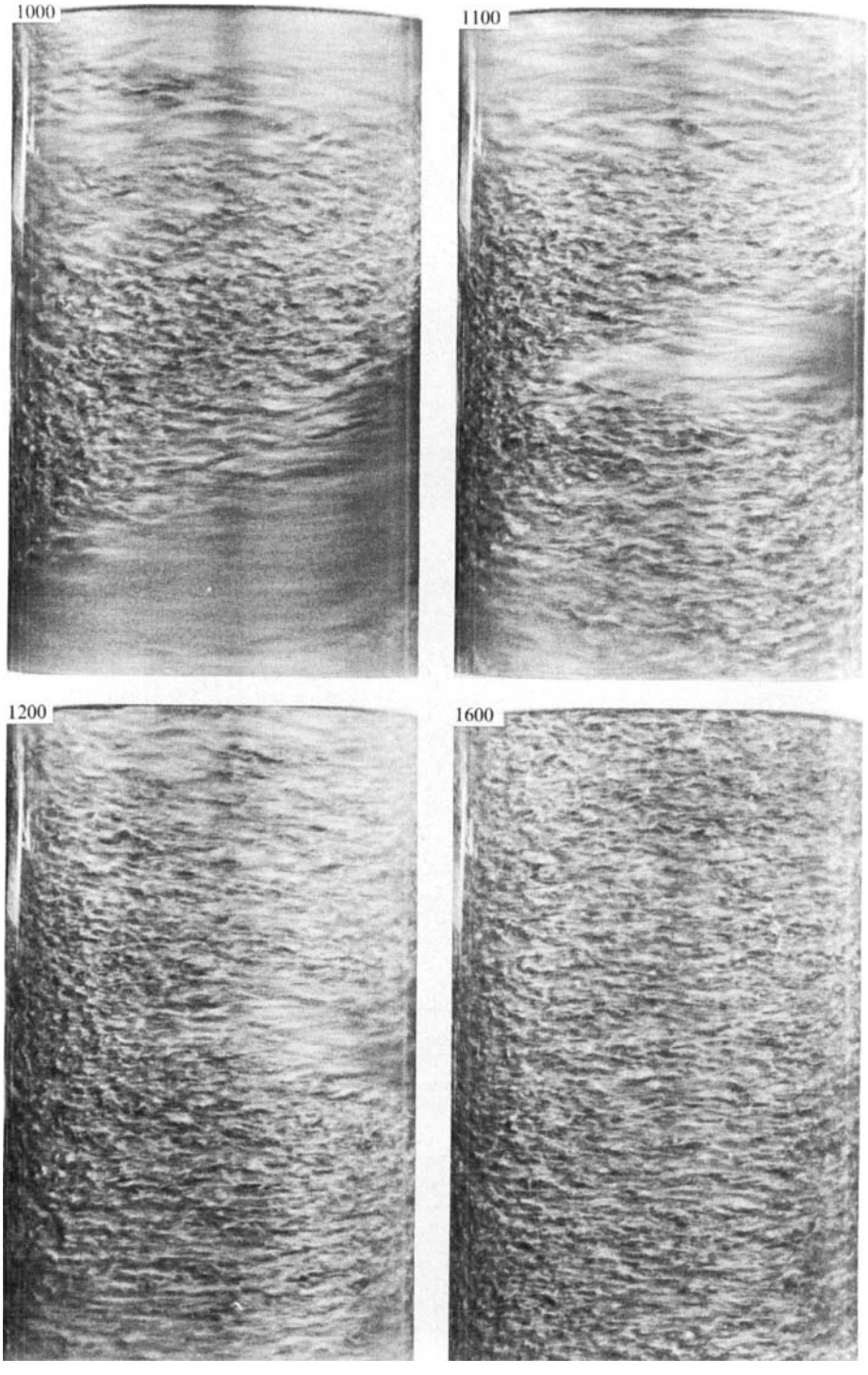

FIGURE 14. Photographic sequence of spiral turbulence (SPT) as R_i was increased for fixed $R_o = -3000$. The numbers on the photographs indicate R_i.

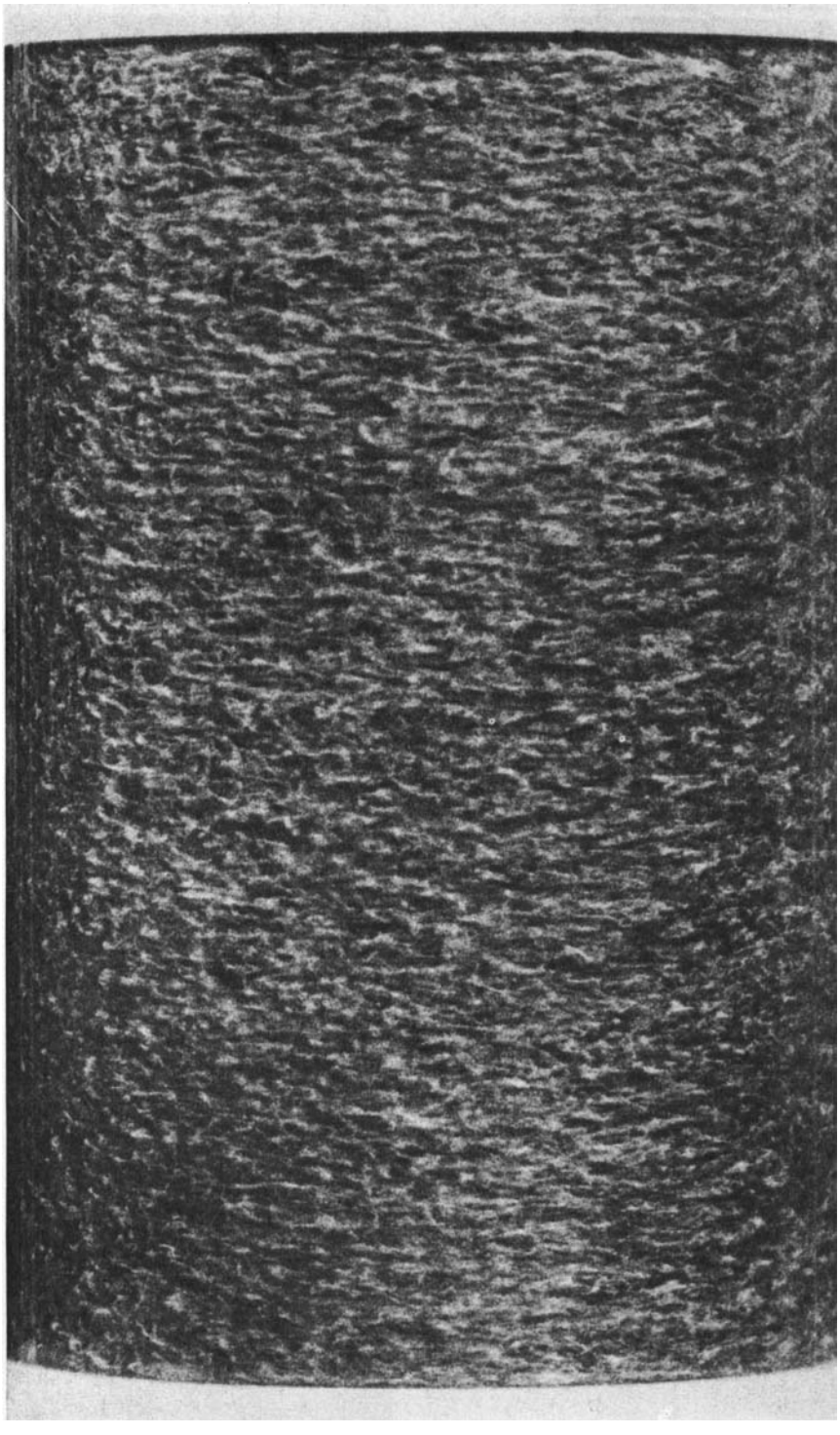

FIGURE 15. Turbulent flow (TUR) at $R_o = -4000$, $R_i = 2000$.

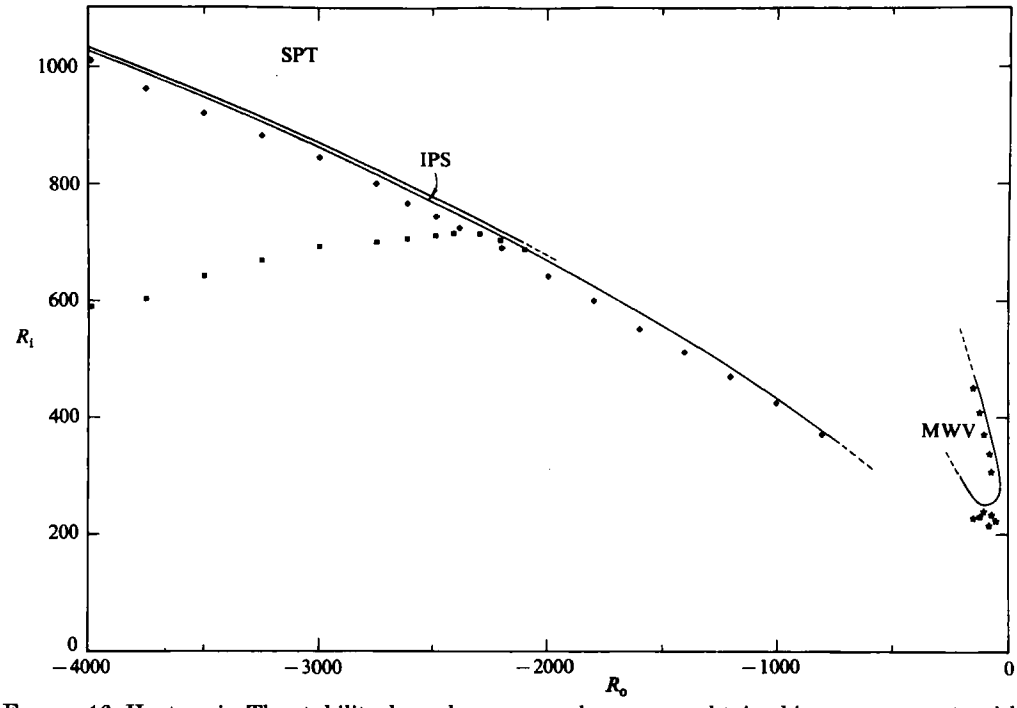

FIGURE 16. Hysteresis. The stability-boundary curves shown were obtained in measurements with R_i *increasing*, as in figure 1. The data points are for *decreasing* R_i: ■, spiral turbulence; ◆, interpenetrating laminar spirals; and ★, modulated wavy vortices.

5. Flow between co-rotating cylinders

The transitions observed in flow between co-rotating cylinders are summarized in figure 18.

5.1. *Basic flow*

The basic flow between co-rotating cylinders is azimuthal, the same as for counter-rotating cylinders. However, for the co-rotating case there is no radius where the velocity goes to zero; therefore, if any region of the flow becomes centrifugally unstable by the Rayleigh criterion, then the flow at all radii is unstable.

End effects are important in understanding the flow near the first instability, perhaps more so than for counter-rotating cylinders. Figures 3(*b*) and (*c*) show the end cells just below Taylor-vortex onset for small and large R_o, respectively. For finite-length cylinders rotating at high speeds the overall flow near the onset of Taylor-vortex flow may be dominated by the end cells. Figure 19 shows that the heights of the end cells at Taylor-vortex onset become many times the gap width at large R_o. With $\Gamma = 30$ the fraction of the total cylinder length that is occupied by the end cells reaches 0.6 within the range of R_o in figure 19; thus in order to examine properly the bulk flows near onset at larger R_o than in the present survey (where $R_o < 1200$) the aspect ratio would have to be increased significantly. However, for R_i well above Taylor-vortex onset in any case the end cells become much smaller; this occurs through a process of successive formation and shedding of Taylor vortices from the end cells as R_i is increased. Thus, if R_i is sufficiently far above the Taylor-vortex onset, it may still be possible to neglect end effects. In all the observations we report in

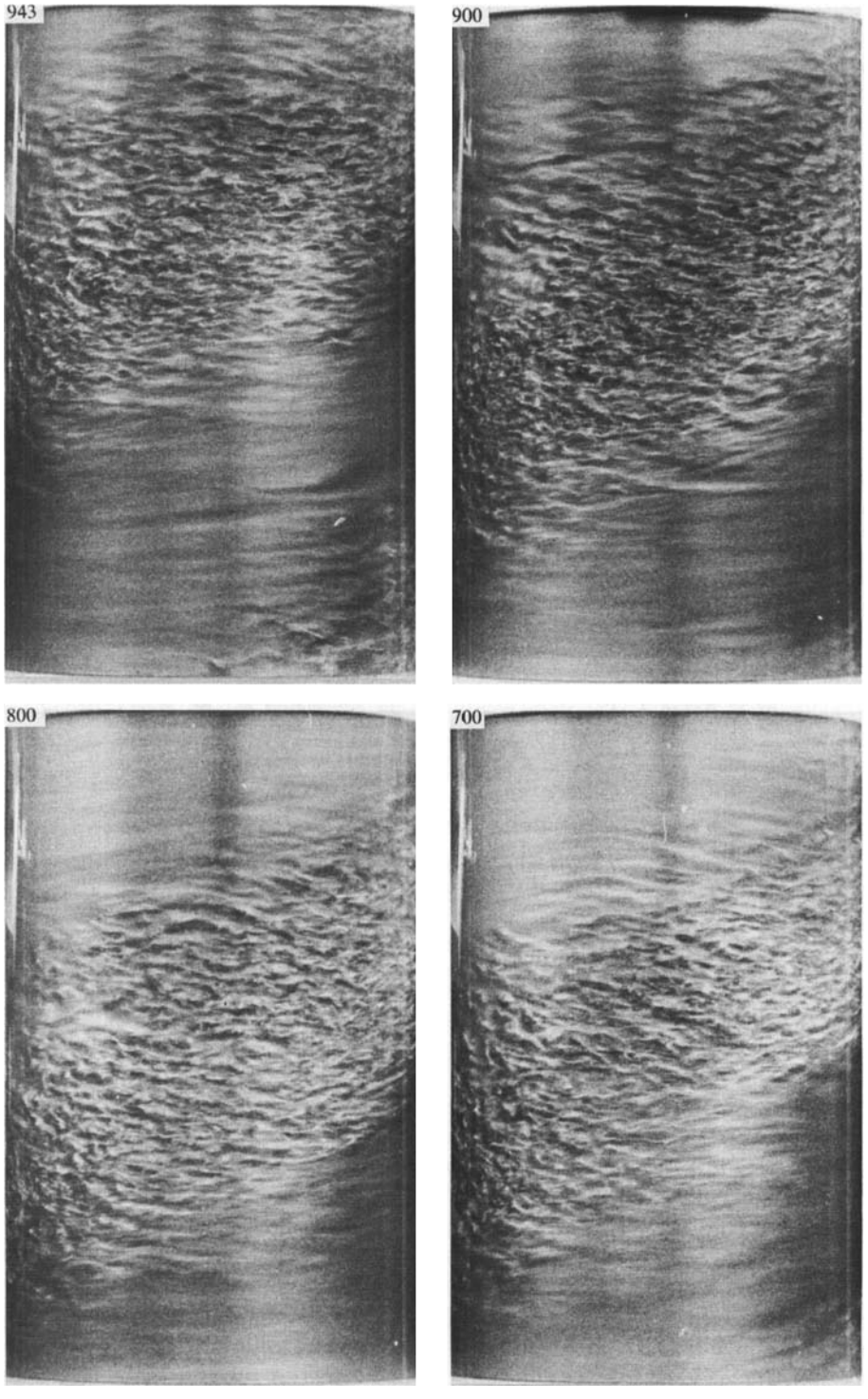

FIGURE 17. These photographs illustrate the hysteresis in spiral turbulence as R_i was decreased below the initial onset value ($R_i = 868$), for $R_o = -3000$. The numbers on the photographs indicate R_i.

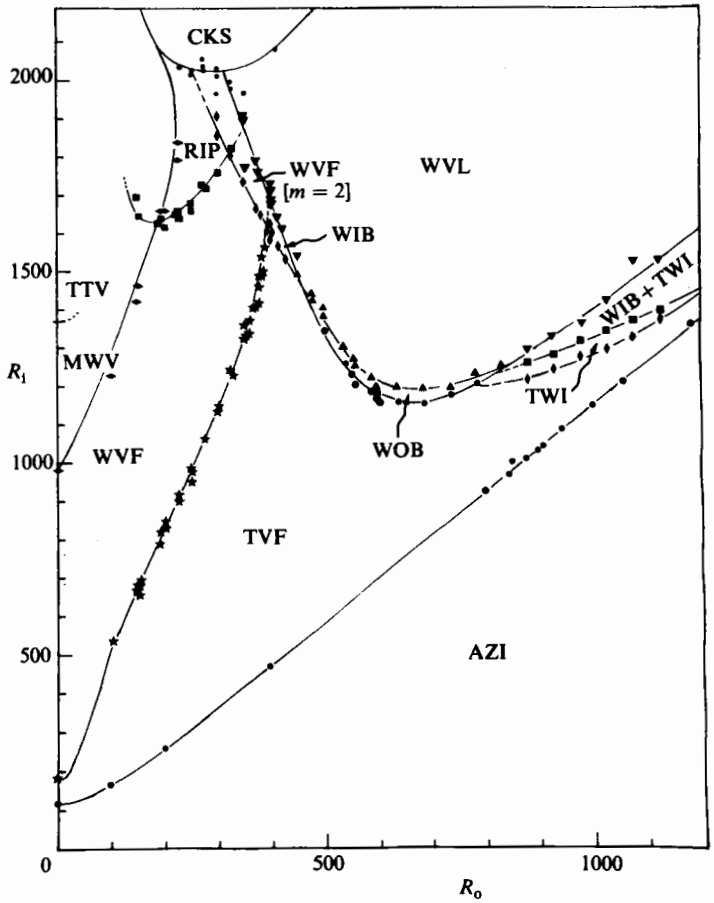

FIGURE 18. The flow-regime diagram for co-rotating cylinders. The abbreviations for the different flows are defined in table 1. The different symbols distinguish data for different transitions.

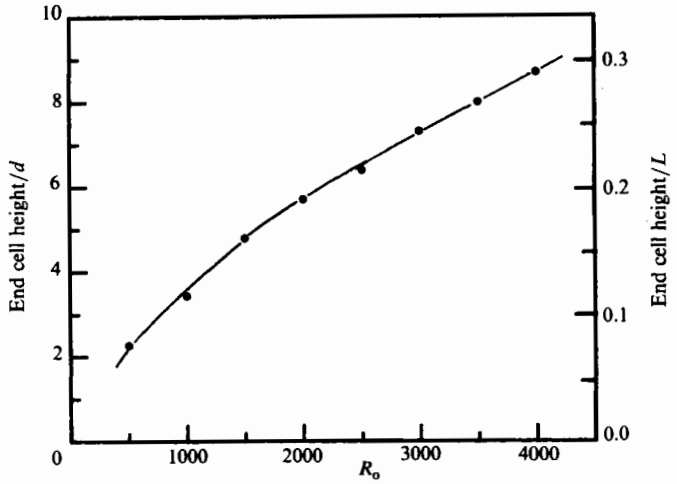

FIGURE 19. End-cell height as a function of R_o at the onset of Taylor-vortex flow for flow between co-rotating cylinders. In the Reynolds-number range of these data the onset of Taylor vortex flow ranges from $R_i = 580$ at $R_o = 500$ to $R_i = 4650$ at $R_o = 4000$. Note that the data in figures 1 and 18 correspond to $R_o \leqslant 1200$; in this range of R_o the ratio of the end cell height to annulus length is less than 0.13 near Taylor-vortex-flow onset and much smaller still at larger R_i.

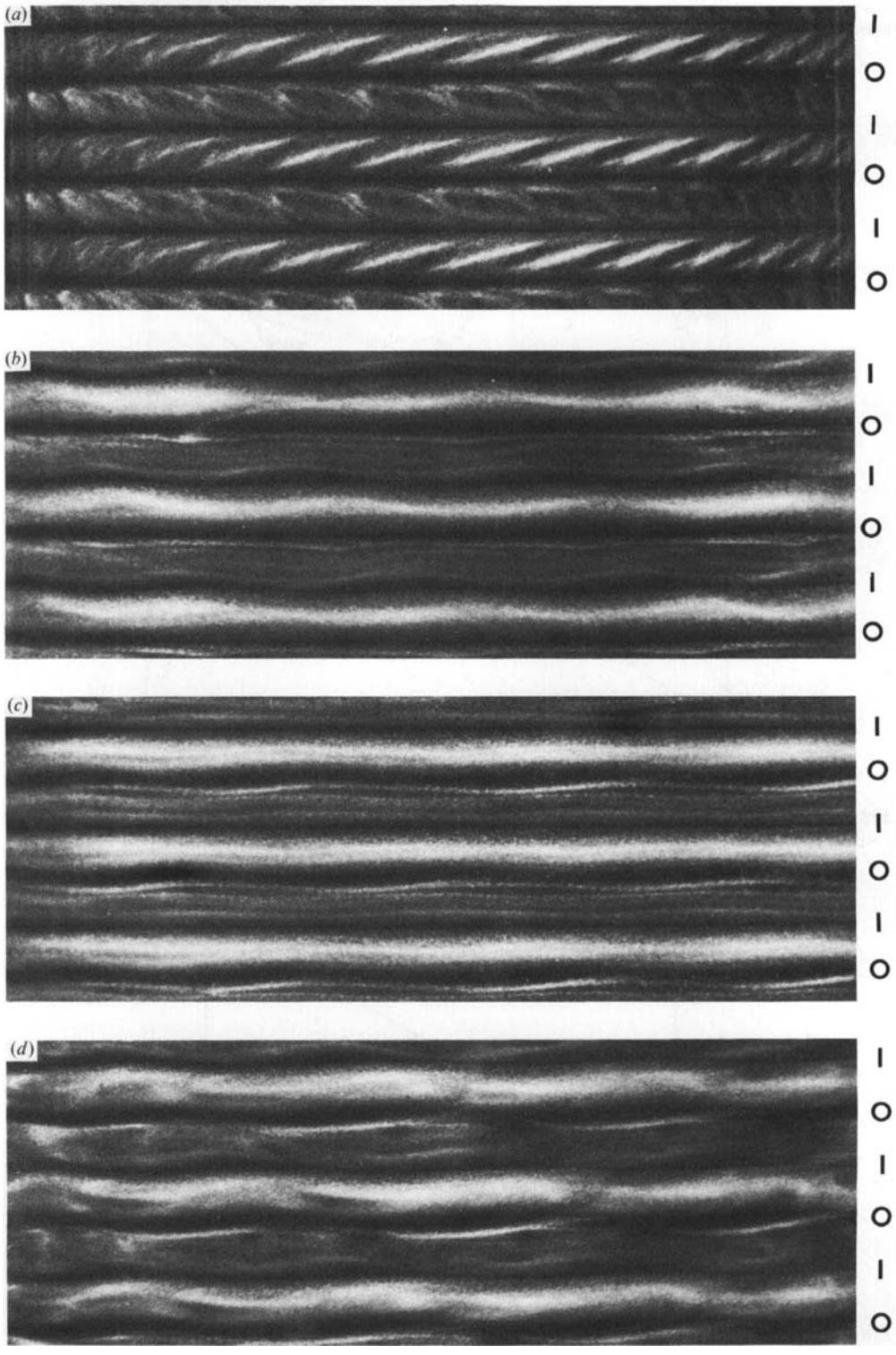

FIGURE 20. (*a*) Twisted Taylor vortices (TWI); $R_i = 1040$, $R_o = 720$. (*b*) Wavy inflow boundaries (WIB); $R_i = 1310$, $R_o = 700$. (*c*) Wavy outflow boundaries (WOB); $R_i = 1170$, $R_o = 700$. (*d*) Wavelets (WVL); $R_i = 1250$, $R_o = 730$. $\Gamma = 30$ for all four cases. The letters I and O indicate the inflow and outflow boundaries, respectively.

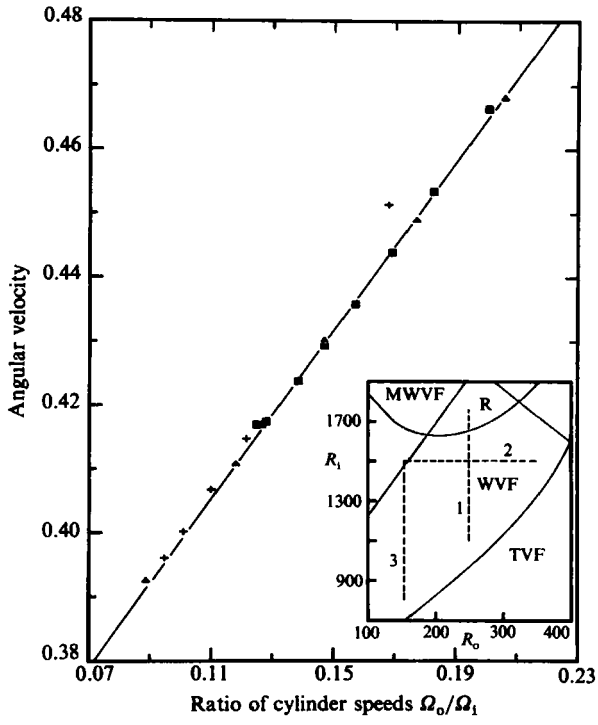

FIGURE 21. The angular velocity of wavy vortex flow between co-rotating cylinders. The solid line is an empirical fitting function, $0.332(1+2\mu)$. The ■s correspond to points on path 1 shown in the inset, the ▲s correspond to points on path 2, and the +s correspond to points on path 3.

§§5.2–5.4 the measurements were made under conditions in which the end cells occupied a small fraction of the cylinder length; hence end effects were neglected.

5.2. *Primary instability*

The azimuthal bulk flow between co-rotating cylinders is unstable to the formation of time-independent Taylor vortices, as indicated by the label TVF in figure 18. This is consistent with the stability analysis of Krueger *et al.* (1966).

5.3. *Twisted vortices*

Visually the most unusual flow between co-rotating cylinders is what we have called twisted vortex flow, found in the region labelled TWI in figure 18. This flow, discussed in Andereck *et al.* (1983), is shown in figure 20(*a*). The pattern consists of a periodic rope-like structure internal to the Taylor vortices; the inflow and outflow boundaries remain flat within observational limits. The axial phase-locking of the pattern indicates that some communication occurs across the vortex boundaries in spite of their flatness. This flow is consistent with the predictions of the bifurcation analyses of Golubitsky & Stewart (1986), Chossat & Iooss (1985), and Demay & Iooss (1984).

5.4. *Wavy vortex boundary flows*

Four distinct simple wavy vortex boundary flows have been found between co-rotating cylinders. The first is wavy vortex flow (WVF in figure 18), in which both the inflow

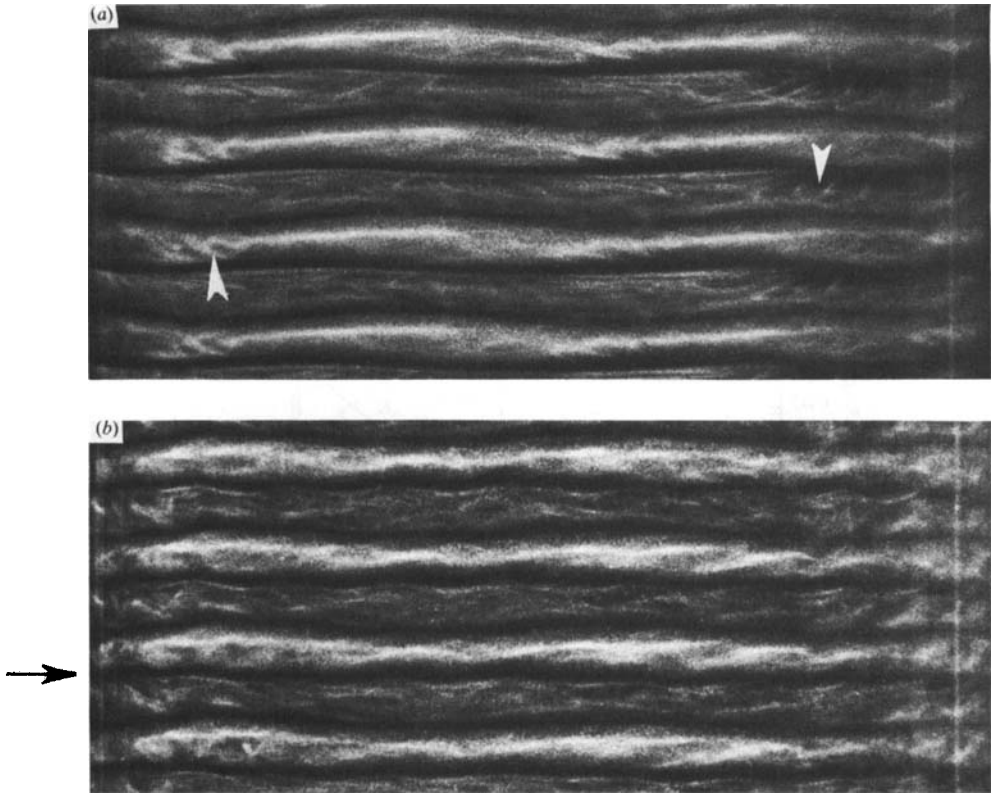

FIGURE 22. (*a*) The arrows point to the 'ripple' (RIP) observed in wavy-Taylor-vortex flow; $R_i = 1750$, $R_o = 250$. (*b*) The arrow points to the 'corkscrew' (CKS) pattern observed on wavy-Taylor-vortex-flow boundaries; $R_i = 2030$, $R_o = 300$. $\Gamma = 30$ in both cases.

and outflow boundaries are wavy, with the same angular velocity for each wave. There are typically 6 waves around the cylinder, although, as can be seen in the flow-regime diagrams, there is a regime in which the wavenumber is as low as 2. The angular velocities of the waves are plotted for several values of R_o and R_i in figure 21.

The wavy inflow- and outflow-boundary flows (WIB and WOB, respectively) are two distinct flows in which one boundary is flat while the other is wavy, as can be seen in figures 20(*b*) and 20(*c*). These patterns have an axial period twice the wavelength of the axisymmetric Taylor vortices. The amplitude of these waves never grows as large as the amplitude of a wavy vortex with similar azimuthal wavenumber. For our choice of axial wavelength the flow with a wavy inflow boundary can co-exist with twists, as noted in the flow-regime diagrams.

The fourth flow, called wavelets (WVL in figure 18) is shown in figure 20(*d*). There are waves on both boundaries, similar in appearance to the waves in WIB and WOB. In contrast to wavy-vortex flow, the waves on the inflow and outflow boundaries for the wavelet flow move at different angular velocities and in general have different azimuthal wavenumbers, as confirmed by observations in a rotating reference frame. This is therefore a quasi-periodic flow that is distinct from the modulated wavy vortex flows discussed in §4.4 and in Gorman & Swinney (1982) and Shaw *et al.* (1982). The wave angular velocities have not yet been determined for this flow. Further details on WIB, WOB, and WVL may be found in Andereck *et al.* (1983).

5.5. *High-azimuthal-wavenumber flows*

For $R_i > 1500$, flows are found with azimuthal wavenumbers considerably higher than for any of the flows discussed thus far. The first of these is a small-amplitude wave which we have termed ripple (labelled RIP in figure 18); it is most noticeable near the narrow region of a wavy vortex, as shown in figure 22(*a*).

At still larger R_i there appears a large wavenumber disturbance associated mainly with the outflow boundaries, although the waves extend from the boundaries around the vortices in a corkscrew fashion; hence the mnemonic CKS in figure 18. This flow feature is indicated by arrows in figure 22(*b*); it may be related to the instability of the vortex outflow-boundary jet discussed by Reith (1981).

6. Discussion

Previous theoretical work has largely dealt with the primary instabilities of Couette flow. For example, Krueger *et al.* (1966) have analysed the behaviour of the system near $R_o = -155$, $R_i = 180$, a region characterized by the intersection of several transition boundaries, and found that the azimuthal flow is unstable to Taylor vortices for $R_o \gtrsim -155$ and to spiral vortices for $R_o \lesssim 155$. More recently, R. C. DiPrima, P. M. Eagles & J. Sijbrand (private communication) have used a numerical approach on a six-dimensional manifold to predict Taylor vortices, spiral vortices, and, as a nearby secondary instability, wavy spirals. Their results are generally in accord with our observations.

Chossat & Iooss (1985), Demay & Iooss (1984) and Golubitsky & Stewart (1986) have examined analytically the bifurcations possible given the symmetries of the system; Golubitsky & Stewart (1986) have in addition made an explicit reduction to a six-dimensional manifold. These authors have obtained solutions consistent with Taylor vortices, wavy vortices, modulated wavy vortices, spiral vortices, and twists.

To understand more fully the various flows and instabilities we have described, particularly those far removed from simple Couette flow, it will be necessary to use a variety of numerical and analytical techniques, as well as to conduct detailed experimental studies of specific flows and the transitions between flows. We now suggest possible directions for future work.

First, it should be possible to investigate many of these flows with numerical techniques such as the pseudo-spectral method used by Marcus (1984*a*, *b*), the Galerkin method used by Jones (1982), and the finite-difference method used by Fasel & Booz (1984) and by Lucke *et al.* (1984). Such numerical simulations will help provide an understanding of the underlying physical processes leading to the different instabilities.

Second, dynamical systems-analysis methods, including phase-portrait reconstruction from time series and subsequent extraction of Poincaré sections and maps, should be applicable to the flows we have discussed. Procedures have been developed for computing from the phase portraits the dimensions of the phase-space attractors (Brandstater *et al.* 1983) and Lyapunov exponents (Wolf *et al.* 1985); use of these procedures will quantify the different chaotic flows.

Third, the flows we have described should be amenable to multiple co-dimension bifurcation analysis (see Guckenheimer 1981, 1984; Arneodo, Coullet & Spiegel 1984; Brand, Hohenberg & Steinberg 1984; Knobloch & Guckenheimer 1983). Of particular interest will be the neighbourhoods of co-dimension-two bifurcation points (where

stability boundaries intersect). It is possible that mode competition in these regions will lead to chaotic behaviour.

Finally, the present experiments have been conducted with one basic procedure (with R_o fixed and R_i increased quasi-statically), one radius ratio ($\eta = 0.883$), and, for co-rotating cylinders, one average axial wavelength ($\bar{\lambda}/d = 2.00$). Changing the parameters or the procedure will significantly affect the flow-regime diagrams, possibly produce new states of flow, and may reveal the presence of bifurcations of co-dimension greater than two.

In summary, the characterization of the various flows described in the present study should serve as a guide to future experimental and theoretical studies of the bifurcations and bifurcation sequences in the circular Couette system.

We thank C. Chen, R. Tagg, and E. Zaidman for assistance in some of the observations. This research was supported by National Science Foundation Fluid Mechanics program Grant MEA82-06889. One of us (H.L.S.) acknowledges the support of a Guggenheim Fellowship.

REFERENCES

Ahlers, G., Cannell, D. S, & Dominguez-Lerma, M. A. 1983 Possible mechanism for transitions in wavy Taylor vortex flow. *Phys. Rev.* A **27**, 1225.

Andereck, C. D., Dickman, R. & Swinney, H. L. 1983 New flows in a circular Couette system with co-rotating cylinders. *Phys. Fluids* **26**, 1395.

Arneodo, A., Coullet, P. H. & Spiegel, E. A. 1985 The dynamics of triple convection. *Geophys. Astrophys. Fluid Dyn.* (In the press.)

Brand, H. R., Hohenberg, P. C. & Steinberg, V. 1984 Codimension-two bifurcations for convection in binary fluid mixtures. *Phys. Rev.* A **30**, 2548.

Brandstater, A., Swift, J., Swinney, H. L., Wolf, A., Farmer, J. D., Jen, E. & Crutchfield, J. P. 1983 Low dimensional chaos in a hydrodynamic system. *Phys. Rev. Lett.* **51**, 1442.

Chossat, P. & Iooss, G. 1985 Primary and secondary bifurcation in the Couette–Taylor problem. *Japan J. Appl. Maths* **2**, 37.

Coles, D. 1965 Transition in circular Couette flow. *J. Fluid Mech.* **21**, 385.

Coles, D. & Van Atta, C. 1966 Measured distortion of a laminar circular Couette flow by end effects. *J. Fluid Mech.* **25**, 513.

Couette, M. 1890 Études sur le frottement des liquides. *Ann. Chim. Phys.* **21**, 433.

Demay, Y. & Iooss, G. 1984 Computation of bifurcated solutions for the Couette–Taylor problem, both cylinders rotating. *J. Méc. Théor. Appl., numéro. spécial*, 193.

DiPrima, R. C. & Swinney, H. L. 1981 Instabilities and transition in flow between concentric rotating cylinders. In *Hydrodynamic Instabilities and the Transition to Turbulence* (ed. H. L. Swinney & J. P. Gollub), p. 139. Springer.

Fasel, H. & Booz, O. 1984 Numerical investigations of supercritical Taylor vortex flow for a wide gap. *J. Fluid Mech.* **138**, 21.

Fenstermacher, P. R., Swinney, H. L. & Gollub, J. P. 1979 Dynamical instabilities and the transition to chaotic Taylor vortex flow. *J. Fluid Mech.* **94**, 103.

Frisch, U. & Morf, R. 1981 Intermittency in nonlinear dynamics and singularities at complex times. *Phys. Rev.* A **23**, 2673.

Golubitsky, M. & Stewart, I. 1986 Symmetry and stability in Taylor–Couette flow. *SIAM J. Math. Anal.* **17**, (in press).

Gorman, M. A. & Swinney, H. L. 1982 Spatial and temporal characteristics of modulated waves in the circular Couette system. *J. Fluid Mech.* **117**, 123.

Greenside, H. S., Ahlers, G., Hohenberg, P. C. & Walden, R. W. 1982 A simple stochastic model for the onset of turbulence in Rayleigh–Bénard convection. *Physica* **5D**, 322.

GUCKENHEIMER, J. 1981 On a co-dimension two bifurcation. *Springer Lecture Notes in Math.* **898**, 99.

GUCKENHEIMER, J. 1984 Multiple bifurcations of co-dimension two. *SIAM J. Math. Anal.* **15**, 1.

JONES, C. A. 1982 On flow between counter-rotating cylinders. *J. Fluid Mech.* **120**, 433.

KING, G. P. & SWINNEY, H. L. 1983 Limits of stability and irregular flow patterns in wavy vortex flow. *Phys. Rev.* A **27**, 1240.

KING, G. P., LI, Y., LEE, W., SWINNEY, H. L. & MARCUS, P. S. 1984 Wave speeds in wavy Taylor vortex flow. *J. Fluid Mech.* **141**, 365.

KNOBLOCH, E. & GUCKENHEIMER, J. 1983 Convective transitions induced by a varying aspect ratio. *Phys. Rev.* A **27**, 408.

KRUEGER, E. R., GROSS, A. & DIPRIMA, R. C. 1966 On the relative importance of Taylor-vortex and non-axisymmetric modes in flow between rotating cylinders. *J. Fluid Mech.* **24**, 521.

LUCKE, M., MILHELCIC, M., WINGERATH, K. & PFISTER, G. 1984 Flow in a small annulus between concentric cylinders. *J. Fluid Mech.* **140**, 343.

MALLOCK, A. 1888 Determination of the viscosity of water. *Proc. R. Soc. Lond.* A **45**, 126.

MALLOCK, A. 1896 Experiments on fluid viscosity. *Phil. Trans. R. Soc. Lond.* A **187**, 41.

MARCUS, P. S. 1984*a* Simulation of Taylor–Couette flow. Part 1. Numerical methods and comparison with experiment. *J. Fluid Mech.* **146**, 45.

MARCUS, P. S. 1984*b* Simulation of Taylor–Couette flow. Part 2. Numerical results for wavy vortex flow with one travelling wave. *J. Fluid Mech.* **146**, 65.

MATISSE, P. & GORMAN, M. 1984 Neutrally buoyant anisotropic particles for flow visualization. *Phys. Fluids* **27**, 759.

OTNES, R. K. & ENOCHSON, L. 1978 *Applied Time Series Analysis.* New York: Wiley.

PARK, K. J. & DONNELLY, R. J. 1981 Study of the transition to Taylor vortex flow. *Phys. Rev.* A **24**, 2277.

PARK, K. J., CRAWFORD, G. L. & DONNELLY, R. J. 1981 Determination of transition in Couette flow in finite geometries. *Phys. Rev. Lett.* **47**, 1448.

REITH, L. A. 1981 Transition to turbulence in a circular Couette system. Ph.D. dissertation, The University of Texas.

SAVAŞ, Ö. 1985 On flow visualization using reflective flakes. *J. Fluid Mech.* **152**, 235.

SHAW, R., ANDERECK, C. D., REITH, L. A. & SWINNEY, H. L. 1982 Superposition of traveling waves in the circular Couette system. *Phys. Rev. Lett.* **48**, 1172.

SNYDER, H. A. 1968*a* Stability of rotating Couette flow. I. Asymmetric waveforms. *Phys. Fluids* **11**, 728.

SNYDER, H. A. 1968*b* Stability of rotating Couette flow. II. Comparison with numerical results. *Phys. Fluids* **11**, 1599.

SNYDER, H. A. 1969 End effects and length effects in rotating Couette flow. Unpublished report.

SNYDER, H. A. 1970 Waveforms in rotating Couette flow. *Intl J. Non-Linear Mech.* **5**, 659.

TAYLOR, G. I. 1923 Stability of a viscous liquid contained between two rotating cylinders. *Phil. Trans. R. Soc. Lond.* A **223**, 289.

VAN ATTA, C. 1966 Exploratory measurements in spiral turbulence. *J. Fluid Mech.* **25**, 495.

WOLF, A., SWIFT, J. B., SWINNEY, H. L. & VASTANO, J. A. 1985 Determining Lyapunov exponents from a time series. *Physica* **16D**, 285.

ZHANG, L. H. & SWINNEY, H. L. 1985 Nonpropagating oscillatory modes in Couette–Taylor flow. *Phys. Rev.* A **31**, 1006.